Creep of lubricated layered nano-porous solids and application to cementitious materials

Matthieu Vandamme, Zdeněk Pavel Bažant, Sinan Keten

Creep of Lubricated Layered Nano-Porous Solids and Application To Cementitious Materials

Matthieu Vandamme[*], Zdeněk P. Bažant[**], and Sinan Keten[***]

[*]Université Paris-Est, Laboratoire Navier (École des Ponts ParisTech, IFSTTAR, CNRS) 6-8 Av. B. Pascal, 77420 Champs-sur-Marne, France
[**]Department of Civil and Environmental Engineering & Department of Mechanical Engineering & Department of Materials Science and Engineering, Northwestern University, 2145 Sheridan Road, Evanston, IL 60208, United States
[***]Department of Civil and Environmental Engineering & Department of Mechanical Engineering, Northwestern University, 2145 Sheridan Road, Evanston, IL 60208, United States

March 18, 2015

Abstract

A variety of geomaterials, such as cementitious or clay-based materials, has on the nano-scale a layered microstructure which can contain fluid in its nano-porous space. The creep of such nano-scale basic units is what causes the macroscopic creep. Here, we study one nano-pore whose walls consist of two parallel infinite solid layers interacting

through Lennard-Jones potential. We evaluate numerically the energy barriers that such a system needs to overcome in order for the two solid layers to slide over each other, and show how this sliding depends on the longitudinal and transverse forces applied to the layers. The energy barriers translate into a dependence of the apparent viscosity of the system on the disjoining pressure, in a manner consistent with the microprestress theory. This result makes it possible to explain why the long-time creep of cementitious materials is logarithmic. We then consider experimental data on how the long-term logarithmic creep of cementitious materials depends on the temperature and relative humidity. Our model can capture the observed dependencies if we take into account not only the energy barriers induced by the interactions between layers, but also the influence of the interlayer fluid, which is water in the case of cementitious materials. We model this fluid as a continuum with the same properties as the bulk fluid.

Introduction

All geomaterials, whether man-made, e.g., cementitious materials in general, or natural, clay-based materials, exhibit creep, i.e., slow deformation over time under the action of sustained mechanical stress. The creep occurs at a rate that can be detrimental to the lifespan of concrete structures and structures on clay foundations [Bažant *et al.* 2011; Puzrin *et al.* 2010]. Cementitious and clay-based materials have in common a phase that confers to

them most of their viscous properties, is nano-porous and layered.

Indeed, the matrix of regular Portland cement paste is made of calcium silicate hydrates (also called C-S-H) which, although spatially variable in both structure and composition [Richardson 1999], consist of more or less ordered stacks of calcium silicate layers, each of which is made of a Ca-O sheet covalently bonded with silicate chains [Richardson 2008; Pellenq *et al.* 2009]. Between those solid calcium silicate layers, one finds a few molecular layers of water.

By contrast, as their name suggests, the minerals in clay-based materials are phyllosilicates made of stacks of layers combining silicate tetahedra with aluminum octahedra [Meunier 2005]. Again, between those solid layers, one finds a few molecular layers of water. Thus the cement-based and clay-based materials share a layered nano-structure which contains interlayer water.

Because the spacing of the adjacent solid layers is on the order of only a nanometer, the clay and C-S-H are subjected to strong disjoining pressures. At the scale of an individual slit nano-pore, the disjoining pressures can lead to swelling or shrinkage during sorption or desorption, and can be not only positive (compression) but also negative (tension). The sign of the disjoining pressure is affected by the ratio of nano-pore width to the number molecular layers of the interlayer fluid in the nano-pore [Ustinov & Do 2006; Bažant & Bazant 2012].

However, when averaged over a distribution of pore sizes in a disordered nano-porous solid (e.g., even in ideal one-dimensional nano-porous solids

[Brochard *et al.* 2012]), one observes during sorption only swelling: In a disordered nano-porous solid, the representative disjoining pressure is positive (i.e., compressive), inducing tensile stresses in the solid microstructure of material (this also means that during desorption one observes only shrinkage). At the macroscopic scale of material, those tensile stresses induced by disjoining pressure and adsorption can reach several dozens of MPa [Espinoza *et al.* 2014]. Locally, those tensile stresses can even be greater, exceeding a hundred of MPa [Bažant 1972].

For both cementitious materials and clay-based materials, various kinetics of creep can be identified. In cementitious materials, a short-term creep kinetics, usually associated with local reorganization of water and lasting from a few weeks to a few years at the macroscopic scale, is followed by a long-term creep kinetics that is logarithmic with respect to time. In clay-based materials and soils in general, the application of load causes water to be expelled (which is the so-called consolidation process [Terzaghi 1996]) but, once the excess fluid pressure is dissipated, soils creep logarithmically with respect to time [Lambe & Whitman 1969].

The origin of this logarithmic creep in both cementitious and clay-based materials has been much disputed. For cementitious materials, an explanation was provided by the so-called microprestress solidification theory [Bažant *et al.* 1997], which recognizes the importance of disjoining pressures and the effect they can have on viscosity. The principle of the theory is the following: The hydration processes in cementitious materials and the restraint induced

by the heterogeneous and disordered microstructure prevent an instantaneous release of the high average tensile disjoining pressure prevailing in the C-S-H nano-pores. This disjoining pressure, acting perpendicularly to the C-S-H layers, will be denoted as S and called microprestress ("nanoprestress" though might be a more accurate term, but the "microprestress" is by now well established). The microprestress initially develops as a consequence of clinker hydration. Later it changes with moisture content and temperature and, in absence of mechanical load on concrete, dominates the stresses in solid microstructure [Bažant *et al.* 1997]. The microprestress theory recognizes that the apparent viscosity (denoted as η) associated with the sliding of two C-S-H layers over each other is sensitive to this microprestress, i.e., $\eta = \eta(S)$. The theory then recognizes that, because of the disordered and isotropic nature of C-S-H at the meso-scale, this microprestress in one layer must induce in layers of different orientation shear forces acting parallel to these layers (see Fig. 1). Based on those features, one can show that, for any power-law dependence of the viscosity on the microprestress (i.e., $\eta \propto 1/S^{p-1}$ with $p - 1 > 0$), the viscosity evolves linearly with time t, i.e., $\eta \propto t$ (see section for a detailed derivation). For a constant stress, we thus obtain a creep rate that declines in proportion to the inverse of time, and thus a creep strain that increases with time logarithmically.

Recognizing the potential role of the enormous tensile stresses induced by disjoining pressures, we aim in the present work at clarifying this role numerically, considering a simplified model system. The system consists

of two solid layers that are parallel to each other, with an interlayer pore space between them. The interlayer fluid is modeled as a continuum, and only an effective potential between atoms of the opposite adjacent layers is introduced. Given their high stiffness [Shahsavari *et al.* 2009; Carrier *et al.* 2014], the solid layers are considered as rigid.

Here we aim at identifying the energy landscape that the system of two layers will be exposed to while sliding over each other. The energy barriers and how they evolve with disjoining pressure effects (i.e., with the micropre-stress) will be translated into the dependence of the apparent viscosity on the microprestress. The relevance of the numerical results with respect to the microprestress theory will be discussed. A comparison with creep data obtained on cementitious materials at various temperatures and relative humidities will be performed.

Shearing of infinite plates interacting through Lennard-Jones potential

We consider two rigid and infinite plates that are parallel to each other. Each plate consists of atoms located on a square lattice (see Fig. 2). All lengths of the problem are made dimensionless by dividing them by the lattice parameter a: Thus, the dimensionless distance between two closest-neighbor atoms within a plate is equal to unity. The two plates are separated by a distance called the basal spacing: Its value, made dimensionless upon division

by the lattice parameter, is denoted as z. The in-plane principal directions of the two plates are considered aligned at all times and are denoted as $\underline{e}_x$ and $\underline{e}_y$; x and y are the dimensionless relative displacements of the top plate with respect to the bottom one in the $\underline{e}_x$ and $\underline{e}_y$ directions, respectively. The origin of the relative displacements is chosen such that the two plates are in an eclipsed configuration when $x = 0$ and $y = 0$.

The i-th atom of one plate interacts with the j-th atom of the other plate through a Lennard-Jones potential:

$$\Psi(r) = \Psi_0 \left[2 \left(\frac{r_0}{r} \right)^{12} - \left(\frac{r_0}{r} \right)^{6} \right], \tag{1}$$

where r is the dimensionless distance between the two atoms, r_0 is the dimensionless equilibrium distance of the Lennard-Jones potential, and Ψ_0 is the depth of the energy well. This interaction potential should be interpreted as an effective one, in the sense that it aims at capturing not only the direct wall-wall interaction, but also the electrostatic and entropic effects due to the presence of the interlayer water, as well as the water-wall interactions. All the energies in the system are made dimensionless by dividing them by the depth of the energy well of this Lennard-Jones potential. Thus, the dimensionless depth of the energy well of the Lennard-Jones potential is equal to unity. Note that, by introducing a characteristic energy (i.e., the depth Ψ_0 of the energy well of the Lennard-Jones potential) and a characteristic length (i.e., the lattice parameter a), we define a characteristic force Ψ_0/a, with respect

to which all forces introduced in the problem will be made dimensionless.

Given the periodicity of the system, all the atoms are equivalent one to the other. Therefore, from now on, we focus on the energy of only one atom of one plate interacting with all the atoms of the other plate. The energy of interaction of this atom is $\sum_i \Psi(r_i)$, where r_i is the dimensionless distance that separates the atom of interest from the atom i in the other plate.

We consider that the atom of interest is subjected to a (dimensionless) force F acting parallel to the layers in the $\underline{e}_x$ direction, and to a (dimensionless) tensile force S normal to the layers, i.e., in the $\underline{e}_z$ direction (this force is the microprestress). Under the action of those forces, the energy E of the atom of interest is:

$$E = \sum_i \Psi(r_i) - Sz - Fx. \tag{2}$$

For a given microprestress S and transversal load F, the energy landscape to which the system is exposed upon a displacement in the $\underline{e}_x$ direction (i.e., upon sliding of the two layers over each other) is obtained as follows. At a given relative displacement x, for a fixed relative displacement $y = 0.5$, the energy E is minimized with respect to the distance z between the two plates (indeed, we checked that, at given x, minimizing the energy with respect to y and z yields $y = \pm 0.5$): Thus, at the given relative displacement x, the equilibrium z-position of the layer is determined, and the energy E of this equilibrium state is stored. This calculation is repeated for a variety

of relative displacements x. Note that, in these calculations, the force S normal to the layers is kept constant: When the relative displacement x evolves, the z-position of the layer (i.e., the interlayer spacing) varies. Said otherwise, shear induces volume variations, as noted by Hoang & Galliero (2015). However, the C-S-H layers being surrounded by the solid C-S-H gel, this variation of the z-position would be partly prevented and thus translate into variations of the force S: Here, we neglect this effect.

The results for a dimensionless equilibrium distance $r_0 = 1$ are displayed in Fig. 3. Calculations for microprestress $S > 6$ were not possible, because such microprestress suffices to separate the two plates from each other. First, one observes that, in absence of any transversal load or microprestress, equilibrium positions are at $x = \pm 0.5$, i.e., when the two plates are in a staggered position with respect to each other. For the plate to be translated from $x = -0.5$ to $x = 0.5$, the system needs to overcome an energy barrier, which we denote as ΔE. In absence of a transversal load F, an increase of the microprestress S decreases this energy barrier. Furthermore, application of a transversal load F imposes on the energy landscape an asymmetric tilt. This induced tilt causes a decrease of the energy barrier that the plate needs to overcome in order to move in the specified direction of the transversal load, and to an increase of the energy barrier that the plate needs to overcome in order to move in the reverse direction. This favors the sliding in the direction of the transversal load.

Based on energy landscapes such as the ones displayed in Fig. 3, one

can calculate how the energy barrier ΔE required for the plate to move by one lattice spacing in the direction of the transversal load evolves with the various loadings. The calculated energy barriers are displayed in Fig. 4. We may distinguish two regimes, at low and high microprestress. When the microprestress is low enough, then, for any transversal load, the energy barrier ΔE decreases linearly with the normal force S, i.e., $\Delta E = c_1 - c_2 S$, where c_1 and c_2 are functions of the transversal load. In contrast, when the microprestress S is high enough, then, for any transversal load F, the energy barrier ΔE decreases linearly with the logarithm of the normal force S, i.e., $\Delta E = c_3 - c_4 \ln(S)$. Again, the coefficients c_3 and c_4 depend on the transversal load.

In an isotropic solid such as C-S-H on the mesoscopic scale, the microprestress S must induce a transversal load F. Reasonably, one can assume that this transversal load will represent a fraction of the microprestress S. For various ratios F/S of the transversal load F to the microprestress S, we plot how the energy barrier for dimensionless equilibrium distance $r_0 = 1$ depends on the microprestress S; see Fig. 5a. For large enough microprestresses S, we observe a clear logarithmic dependence of the energy barrier on the microprestress S, i.e. $\Delta E = \alpha_1 - \alpha_2 \ln(S)$. Interestingly, to first order, the coefficient α_2 does not depend on the ratio F/S. Therefore, independent of this ratio (which we do not know, as it is a consequence of the spatial orientation of the microstructure, of the elastic properties of the phases, and of the hydration process), the energy barrier ΔE decreases linearly with the

logarithm of the stresses.

Over this latter range of large enough microprestress, when introducing an Arrhenius-type dependence of viscosity on the energy barrier [Debenedetti & Stillinger 2001; Nabarro 2001], i.e.,

$$\eta \propto \exp(\Delta E/k_B T)), \tag{3}$$

we find, for the apparent viscosity η associated to the sliding of the two layers over each other, the following relation:

$$\eta \propto \exp\left(\frac{\alpha_1 - \alpha_2 \ln(S)}{k_B T}\right) = \exp\left(\frac{\alpha_1}{k_B T}\right)\left(\frac{1}{S}\right)^{\alpha_2/k_B T}. \tag{4}$$

Since $\eta \propto 1/S^{p-1}$ with $p-1>0$, we thus observe, for large microprestress, a dependence of viscosity on microprestress that can justify the microprestress theory (see section).

In terms of orders of magnitude, we find out that the dimensionless energy barriers ΔE are on the order of unity (see Fig. 4). It follows that the energy barriers are on the order of Ψ_0 and thus, classically for Lennard-Jones potentials, on the order of 10^{-21} J. Those energy barriers are therefore of the same order of magnitude as $k_B T \approx 10^{-21}$ J at $T = 300$ K. Therefore, the proposed mechanism of a viscosity affected by the energy barriers due to the effective wall-wall interaction is plausible. In terms of stresses at stake, the dimensionless normal forces considered in the study are on the order of unity as well (see Fig. 4), i.e., the normal forces are on the order of Ψ_0/a. Those

normal forces translate into normal stresses on the order of Ψ_0/a^3, i.e., into normal forces on the order of 1 eV / $(1\text{ nm})^3 \approx 10^8$ Pa = 100 MPa. Therefore, the characteristic stresses considered in this study are on the order of the stresses induced by disjoining pressures in real systems.

The fact that the model nano-scale system we here propose (see Fig. 2) makes it possible to retrieve the micoprestress theory, and hence a long-term creep of cementitious materials that evolves with time as a logarithmic function, may look surprising at first glance. Indeed, C-S-H layers are made of several chemical elements and are complex chemically. Therefore, with respect to natural C-S-H, or even to already existing C-S-H molecular models (see, e.g., Taylor (1986); Richardson (2008); Pellenq *et al.* (2009)), our model is crude, in the sense that it fully neglects the chemistry of C-S-H. The fact that, in spite of this crudeness, our system makes it possible to retrieve the microprestress theory, shows that the logarithmic feature of long-term creep of cementitious materials does not originate from any chemical specificity of C-S-H. Such a conclusion is consistent with the experimental observation that clays also creep logarithmically with respect to time in the long term, although the chemical composition of the clay layers differs from the chemical composition of C-S-H. In contrast, the feature that our system keeps in common with C-S-H is that it is a nano-porous layered material. This observation hints towards a logarithmic creep of cementitious materials that would originate from the fact that C-S-H is a nano-porous layered material.

Dependence of viscosity on microprestress, temperature and water content

The model we have formulated allows us to deduce a dependence of viscosity on microprestress that is consistent with the microprestress theory. We now aim at determining whether this model makes it possible to retrieve the observed dependence of creep of cementitious materials on water content and temperature. Since this model makes it also possible to retrieve a creep that evolves logarithmically with respect to time, the comparison with experimental data for cementitious materials is restricted to the long-term creep, which does evolve logarithmically with respect to time. To compare our model with the existing data, we first review the main steps of the derivation of the microprestress theory, as presented next.

Dependence on temperature

Let us now focus on the effect of temperature on the viscosity predicted by our model, and on the consistency of this prediction with the phenomenology of long-term creep of cementitious materials. The derivation of the microprestress theory proceeds as follows [Bažant *et al.* 1997]:

The shear stress, τ, applied to the C-S-H layers may be expressed as $\tau = \eta\dot{\epsilon}$ where η is the viscosity, ϵ is the shear strain, and $\dot{\epsilon}$ is the shear strain rate, which characterizes the sliding of the two parallel layers over each other. The relaxation of the microprestress S is imagined to be the result of a creep

(or flow) of similar origin, resisted by a spring of stiffness K_S coupled in series, as sketched in Fig. 1. Thus, the equation governing the relaxation process is:

$$\frac{\dot{S}}{K_S} + \frac{S}{\eta(S)} = 0. \tag{5}$$

The viscosity must depend on the microprestress S, and since no characteristic value of this dependence is known, the dependence must be self-similar, i.e., a power law:

$$\eta = \frac{1}{\alpha}\frac{1}{S^{p-1}} \text{ (with } p > 1), \tag{6}$$

where p and α are constants. Differential equation (5) may then be solved and one gets $S^{1-p} = \alpha K_S(p-1)t$. The evolution of the viscosity with time then follows:

$$\eta = K_S(p-1)t. \tag{7}$$

By comparing Eq. (6) with Eq. (4), we find that $p - 1 = -\alpha_2/(k_B T)$.

At the scale of a macroscopic concrete specimen, a constant uniaxial stress σ_u is thus expected to cause the axial strain rate $\dot{\epsilon_u} \propto \sigma_u/\eta$. Therefore, the material compliance $\dot{J}_u = \dot{\epsilon_u}/\sigma_u$ defining the creep is expected to evolve as:

$$\dot{J}_u \;\propto\; \frac{1}{\eta} \;=\; \frac{k_B T}{K_S \alpha_2}\,\frac{1}{t}. \tag{8}$$

This equation shows that, as anticipated, the power-law dependence (4) of the viscosity on the microprestress translates into a creep rate that decreases as $1/t$. Therefore, after integration, one finds that the long-term creep evolves

logarithmically with respect to time.

From Eq. (8), one may expect that the rate of this long-term logarithmic creep should scale linearly with the temperature T. Said otherwise, the parameter $c_u = t\dot{J}_u$, which is independent of time when the creep is logarithmic, should be proportional to the temperature T. For a few concrete specimens, for which the basic creep (i.e., the creep at no moisture exchange) has been measured at various temperatures (see the data in Nasser & Neville (1965); York *et al.* (1970); Kommendant *et al.* (1976), gathered in Bažant *et al.* (2004)), we display in Fig. 6a the parameter $c_u = t\dot{J}_u$ as obtained by the optimal fitting of creep data in the range within which the creep was actually logarithmic in time. From the experiments, we find that the parameter $c_u = t\dot{J}_u$ is not proportional to the temperature T.

A reason for this more complex scaling can be found in the behavior of the interlayer water, the effect of which we have for now discarded. Indeed, for the two C-S-H layers to slide over each other, we need not only to displace the two layers respectively to each other, but we also need to shear the interlayer water. In the numerical study performed in Sec. , the calculated energy barriers are those corresponding only to the relative displacement of the two C-S-H layers. Those energy barriers can be modified by the presence of water (as will be seen in Sec.), as interlayer water screens the interactions between the C-S-H layers, but this screening is only a consequence of the *presence* of the interlayer water, not of its *shearing*, the contribution of which does therefore not appear explicitly in Eq. (8). However, on top of the contribution

of the energy barriers, the strain rate at which the C-S-H layers slide on each other must also depend on the viscosity η_w of the interlayer water. In fact, the strain rate and the viscosity of the interlayer water should be inversely proportional to each other. An analogy to justify why it should be so is that of a horse that runs erratically and encounters fences on his way, over which he has a given probability of succeeding in jumping; The average speed at which the horse will move away from his starting point will depend on both his true speed (which is the analogous of the inverse of the interlayer water viscosity) and this probability: If the probability for him to succeed in jumping over the fences does not change, if he runs twice as fast, on average he will reach a given distance twice as fast. This observation makes it possible to formulate the unknown proportionality factor in the scaling relation (8), which can be rewritten as:

$$\dot{J}_u \propto \frac{1}{\eta_w} \frac{k_B T}{K_S \alpha_2} \frac{1}{t}, \tag{9}$$

where η_w is the viscosity of the interlayer water. To check the validity of this modified scaling relation, we use the experimental data displayed in Fig. 6a to plot the parameter $t\dot{J}_u\eta_w/T$. The viscosity $\eta_w(T)$ of the interlayer water is approximated by the viscosity of bulk water: Its values at various temperatures are obtained from the NIST standard reference data (http://webbook.nist.gov/chemistry/fluid/). Interestingly, one observes in this figure no specific trend of the parameter $t\dot{J}_u\eta_w/T$ with respect to tem-

perature: For a given concrete, this parameter remains roughly constant.

The foregoing observation validates a model for the creep of layered C-S-H which in essence consists of two mechanisms: 1) interactions between adjacent C-S-H solid layers, which induce energy barriers that need to be overcome, and 2) viscosity of the interlayer fluid itself, which we model as a continuum with properties identical to those of the bulk fluid. The fact that such a model enables us to capture reasonably well the dependence of long-term creep on temperature can seem surprising, since in this model the interlayer water is considered as bulk water, while the physical properties of confined and bulk water are known to differ significantly from each other: For instance, some find out that, for hydrophilic surfaces, the viscosity of confined or interfacial water differs from the viscosity of bulk water by a factor of about 3 [Raviv *et al.* 2001; Sendner *et al.* 2009]. However, note that the relative dependence of the viscosity of confined and bulk water on temperature might be quite similar, in which case the parameter $t\dot{J}_u\eta_w/T$ (see Fig. 6b) would still remain constant with temperature if η_w was the actual viscosity of the confined interlayer water.

Dependence on relative humidity or water content

We now proceed to investigate the effect of relative humidity or water content on the viscosity, as predicted by our model, and the compatibility of this prediction with the phenomenology of long-term creep of cementitious materials. In our model, we will consider that the depth of the energy well

does not vary upon when the water content increases, and that the only aspect that varies is the equilibrium spacing between the two solid plates. In other words, to model an intake of water in the interlayer space, only the equilibrium distance r_0 in the interaction potential (1) is modified, but not the depth Ψ_0 of the energy well.

The energy barriers calculated for various equilibrium distances and under various loadings are depicted in Fig. 5. As already observed in section where calculations are performed for an equilibrium distance $r_0 = 1$, the energy barriers for all equilibrium distances considered decrease, at large microprestress, linearly with the logarithm of the microprestress. They do so at a rate that is independent of the ratio F/S. However, this rate of decrease depends on the equilibrium distance, as can be observed in Fig. 7, which shows the coefficient $-dE/d(\ln S) = \alpha_2$ calculated for the range of high microprestress.

The goal now is to compare our calculations with the experimental data on how creep at moisture equilibrium varies with the relative humidity. To do so, we use data by Zhang (2014), who performed microindentations on compacted specimens of C-S-H powders equilibrated at various relative humidities. Using micromechanics, they back-calculated the creep properties of the C-S-H particles. The creep properties he measured by indentation are condensed into the so-called contact creep modulus C [Vandamme & Ulm 2009]. Zhang et al. showed that this creep modulus is inversely proportional to the parameter $c_u = t\dot{J}_u$ [Zhang *et al.* 2014], which is constant during

the logarithmic long-term creep of cementitious materials. Their results are presented in Fig. 8a.

At the various constant relative humidities considered, the water content is found from the data obtained by Feldman (1973) and reanalyzed by Jennings in the form of adsorption isotherms of C-S-H [Jennings 2008] (see Fig. 8b). To prepare their specimens, Zhang et al. dried the C-S-H powder that they manufactured, rewetted the powder to compact the specimens, and then equilibrated the compacted specimens at the desired relative humidity. Here we consider the second drying isotherm among the isotherms collected by Jennings.

In the driest state possible (i.e., when all evaporable water has left C-S-H), the stoichiometric formula for C-S-H is considered to be $C_{1.7}$-S-$H_{1.3}$ (in cement chemistry notation). Thus its molar mass is equal to 178.84 g.mol^{-1}. In this driest state possible, the structure of C-S-H is considered to be close to that of tobermorite 9 Å, as provided by Bonaccorsi & Merlino (2005) and recalled by Richardson (2008), i.e., orthorombic space group Fd2d with $a = 11.16$ Å, $b = 7.32$ Å, $c = 37.40$ Å, $\alpha = 90°$, $\beta = 90°$, and $\gamma = 90°$.

To approximate this structure with our simple model, we consider that the characteristic spacing between the closest inhomogeneities within each C-S-H layer is $\sqrt{11.16 * 7.32} = 9.03$ Å, and that the basal spacing is $37.40/4 = 9.35$ Å. In this driest state, the thickness of the interlayer water is considered to be null. At larger water contents, we consider that the interlayer space is filled with bulk water, the molar volume of which is 18.048 cm^3.mol^{-1} at 20°C and

0.1 MPa (these data are taken from the NIST standard reference available at http://webbook.nist.gov/chemistry/fluid/). By a simple geometric calculation, we can thus determine how the mass density of C-S-H (or its basal spacing) should be related to its water content.

The result of this calculation is shown in Fig. 8c, along with the states of Jenning's CM-II model for C-S-H [Jennings 2008]. The good agreement observed indicates that the simple way we used to relate the basal spacing (or density) of C-S-H to its water content provides reasonable results. In conjunction with the adsorption isotherm shown in Fig. 8b, these results make it possible to calculate how the basal spacing of C-S-H must have depended on the relative humidity in the experiments of Zhang et al. Since we work with dimensionless data, comparison with our model requires that the basal spacing be made dimensionless by dividing it by the characteristic length 9.03 Å calculated above for tobermorite 9 Å.

As shown by Eq. (8), the presence of the energy barriers that limit, during the logarithmic creep, the sliding of the C-S-H layers over each other causes that function $c_u = t\dot{J}_u$ should scale as:

$$c_u \;=\; t\dot{J}_u \propto \frac{1}{\alpha_2} \;\propto\; -\frac{1}{dE/d(\ln S)} \tag{10}$$

Again, as written in section , this contribution of the energy barriers must be augmented by the contribution of the interlayer water. Note that we consider the viscosity of the interlayer water not to depend on the layer thickness

(i.e., the interlayer water to behave like bulk water). Thus, in absence of any energy barrier induced by the interactions between the adjacent C-S-H layers, the apparent viscosity η associated with the sliding of the C-S-H layers over each other must scale linearly with the inverse $1/d_w$ of the thickness d_w of the interlayer water. Here, as calculated in the previous paragraph, d_w is equal to the basal spacing from which 9.35 Å must be subtracted. Therefore, the foregoing equation must be modified as:

$$t\dot{J}_u \;\propto\; -\frac{d_w}{dE/d(\ln S)} \tag{11}$$

The experimental data of Zhang, together with the prediction by the above equation, are displayed in Fig. 8d, in which the two sets of values are made dimensionless by dividing them by their value at the relative humidity of 11%. Below the relative humidity of 60%, the model is in very good agreement with the set of experimental data, which is very satisfactory given the simplicity of the model. As was the case for the dependence on temperature (see Sec.), such good agreement of the model with experimental data can be surprising, since the actual viscosity of the confined interlayer water differs from that of bulk water, as it depends on confinement, i.e., on the water content. However, the crudeness of this approximation is somewhat comparable to the crudeness of the assumption that the depth of the energy well does not vary upon an increase of water content. Indeed, for hydrophilic surfaces, according to Raviv *et al.* (2001) and Sendner *et al.* (2009), the viscosity of

confined or interfacial water does not differ from the viscosity of bulk water by orders of magnitude but by a factor of about 3.

Above a relative humidity of 60%, our model overestimates the experimental data, and this overestimation increases with the relative humidity. This discrepancy can probably be explained, at least partly, by the fact that the adsorption isotherm used here (see Fig. 8b) takes into account not only the water in the C-S-H interlayers, but also the water adsorbed at the surface of the C-S-H globules [Jennings 2008]: Therefore, the adsorption isotherm considered here overestimates the amount of water contained solely in the C-S-H interlayers. Other candidates to explain the discrepancy are the assumptions of the independence of the viscosity of interlayer water and of the depth of the energy well on confinement.

In any case, in spite of the discrepancy observed at large relative humidity, our model makes it possible to capture remarkably well how the long-term logarithmic creep of C-S-H depends on relative humidity below 60%. We recall that our model takes into account both the influence of the interactions between adjacent C-S-H layers and of the viscosity of the interlayer fluid (considered as a bulk fluid).

Conclusions

1. A model nano-scale system, made of two parallel solid layers separated by interlayer fluid, is a useful representative of the creep-generating mi-

croscopic building blocks in clay-based materials and in calcium silicate hydrates (i.e., C-S-H —the main hydration product in regular Portland cement).

2. The creep may be modeled by atomic interactions between two solid layers subjected to shearing that causes the energy barriers to be overcome and thus the two layers to slide over each other. The evolution of these energy barriers in presence of disjoining pressures and shear stresses can be studied numerically.

3. When the disjoining pressures and shear forces are considered proportional to each other, the energy barriers decrease linearly with the logarithm of the disjoining pressure, and they do so at a rate that is independent of the ratio between disjoining pressures and shear forces (see Fig. 5).

4. This behavior is consistent with the microprestress theory, which makes it possible to explain why, in cementitious materials, the long-term creep evolves in time as a logarithmic function. The logarithmic feature of long-term creep of cementitious materials does not originate from a chemical specificity of C-S-H, but could originate from the fact that, at the nanometric scale, C-S-H is a nano-porous layered material.

5. The analysis of experimental data on the long-term logarithmic creep of cementitious materials, with a focus on the creep kinetics, shows

that the present model system is able to predict the observed effects of temperature (Sec.) and relative humidity (Sec.), provided that one takes into account: 1) the energy barriers that need to be overcome in order for the two solid layers to slide over each other, and 2) the viscosity of the interlayer fluid. In particular, it is possible to fit the test data while considering the interlayer fluid (i.e., water in this study) to behave like a bulk fluid.

6. Although this study is focused on the cementitious materials (i.e., concrete), it can likely be extended to geomaterials such as clays and clay-based materials, in which the basic microscopic building units are also made of solid layers (i.e., phyllosilicates in the case of clay) with interlayer fluid. Indeed, clay-based materials are also known to creep logarithmically in the long term [Lambe & Whitman 1969].

References

Bažant, Zdeněk P. 1972. Thermodynamics of interacting continua with surfaces and creep analysis of concrete structures. *Nuclear engineering and design*, **20**, 477–505.

Bažant, Zdeněk P., & Bazant, Martin Z. 2012. Theory of sorption hysteresis in nanoporous solids: Part I Snap-through instabilities. *Journal of the Mechanics and Physics of Solids*, **60**(9), 1644–1659.

Bažant, Zdeněk P., Hauggaard, Anders Boe, Baweja, Sandeep, & Ulm, Franz-Josef. 1997. Microprestress-solidification theory for concrete creep. I: Aging and drying effects. *Journal of Engineering Mechanics*, **123**(11), 1188–1194.

Bažant, Zdeněk P., Cusatis, Gianluca, & Cedolin, Luigi. 2004. Temperature effect on concrete creep modeled by microprestress-solidification theory. *Journal of engineering mechanics*, **130**(6), 691–699.

Bažant, Zdeněk P., Hubler, Mija H., & Yu, Qiang. 2011. Pervasiveness of excessive segmental bridge deflections: Wake-up call for creep. *ACI Structural Journal*, **108**(6), 767–774.

Bonaccorsi, E., & Merlino, S. 2005. Modular microporous minerals: cancrinite-davyne group and CSH phases. *Reviews in mineralogy and geochemistry*, **57**(1), 241–290.

Brochard, Laurent, Vandamme, Matthieu, & Pellenq, Roland J.-M. 2012. Poromechanics of microporous media. *Journal of the Mechanics and Physics of Solids*, **60**(4), 606–622.

Carrier, Benoit, Vandamme, Matthieu, Pellenq, Roland J.-M., & Van Damme, Henri. 2014. Elastic properties of swelling clay particles at finite temperature upon hydration. *The Journal of Physical Chemistry C*, **118**(17), 8933–8943.

Debenedetti, Pablo G., & Stillinger, Frank H. 2001. Supercooled liquids and the glass transition. *Nature*, **410**(6825), 259–67.

Espinoza, David N., Vandamme, Matthieu, Pereira, J.-M., Dangla, Patrick, & Vidal-Gilbert, Sandrine. 2014. Measurement and modeling of adsorptiveporomechanical properties of bituminous coal cores exposed to CO2: Adsorption, swelling strains, swelling stresses and impact on fracture permeability. *International Journal of Coal Geology*, **134-135**(Nov.), 80–95.

Feldman, R. F. 1973. Helium flow characteristics of rewetted specimens of dried hydrated Portland cement paste. *Cement and Concrete Research*, **3**, 777–790.

Hoang, Hai, & Galliero, Guillaume. 2015. Couplings between swelling and shear in saturated slit nanopores: A molecular simulation study. *Physical Review E*, **91**(1), 012401.

Jennings, Hamlin M. 2008. Refinements to colloid model of C-S-H in cement: CM-II. *Cement and Concrete Research*, **38**(3), 275–289.

Kommendant, G. J., Polivka, M., & Pirtz, D. 1976. *Study of concrete properties for prestressed concrete reactor vessels, final report-part II, Creep and strength characteristics of concrete at elevated temperatures.* Tech. rept. Dept. Civil Engineering, Univ. of California, Berkeley.

Lambe, T. W., & Whitman, R. W. 1969. *Soil mechanics.* Wiley.

Meunier, Alain. 2005. *Clays.* Springer.

Nabarro, F. R. N. 2001. The time constant of logarithmic creep and relaxation. *Materials Science and Engineering A*, **309-310**, 227–228.

553 Nasser, K. W., & Neville, A. M. 1965. Creep of concrete at elevated temper-
554 atures. *ACI Journal Proceedings*, **62**(12), 1567–1579.

555 Pellenq, Roland J.-M., Kushima, Akihiro, Shahsavari, Rouzbeh, Van Vliet,
556 Krystyn J., Buehler, Markus J., Yip, Sidney, & Ulm, Franz-Josef. 2009. A
557 realistic molecular model of cement hydrates. *Proceedings of the National*
558 *Academy of Sciences of the United States of America*, **106**(38), 16102–7.

559 Puzrin, Alexander M., Alonso, Eduardo E., & Pinyol, Núria. 2010. Unex-
560 pected excessive settlements: Kansai international airport, Japan. *Chap.*
561 *2, pages 23–43 of: Geomechanics of Failures*. Dordrecht: Springer Nether-
562 lands.

563 Raviv, U., Laurat, P., & Klein, J. 2001. Fluidity of water confined to sub-
564 nanometre films. *Nature*, **413**(6851), 51–54.

565 Richardson, Ian G. 1999. The nature of C-S-H in hardened cements. *Cement*
566 *and Concrete Research*, **29**(8), 1131–1147.

567 Richardson, Ian G. 2008. The calcium silicate hydrates. *Cement and Concrete*
568 *Research*, **38**(2), 137–158.

569 Sendner, Christian, Horinek, Dominik, Bocquet, Lyderic, & Netz, Roland R.
570 2009. Interfacial water at hydrophobic and hydrophilic surfaces: Slip,
571 viscosity, and diffusion. *Langmuir*, **25**(18), 10768–10781.

572 Shahsavari, R., Buehler, Markus J., Pellenq, Roland J.-M., & Ulm, Franz-
573 Josef. 2009. First-principles study of elastic constants and interlayer inter-

574 actions of complex hydrated oxides: case study of tobermorite and jennite.
575 *Journal of the American Ceramic Society*, **92**(10), 2323–2330.

576 Taylor, H. F. W. 1986. Proposed structure for calcium silicate hydrate gel.
577 *Journal of the American Ceramic Society*, **69**, 464–467.

578 Terzaghi, Karl. 1996. *Soil mechanics in engineering practice*. John Wiley &
579 Sons.

580 Ustinov, E. A., & Do, D. D. 2006. Effect of adsorption deformation on ther-
581 modynamic characteristics of a fluid in slit pores at sub-critical conditions.
582 *Carbon*, **44**(13), 2652–2663.

583 Vandamme, Matthieu, & Ulm, Franz-Josef. 2009. Nanogranular origin of
584 concrete creep. *Proceedings of the National Academy of Sciences of the*
585 *United States of America*, **106**(26), 10552–10557.

586 York, G. P., Kennedy, T. W., & Perry, E. S. 1970. *Experimental investigation*
587 *of creep in concrete subjected to multiaxial compressive stresses and ele-*
588 *vated temperatures*. Tech. rept. Dept. of Civil Engineering, Univ. of Texas,
589 Austin, Tex.

590 Zhang, Qing. 2014. *Creep properties of cementitious materials: effect of*
591 *water and microstructure. An approach by microindentation*. Ph.D. thesis,
592 Université Paris-Est.

593 Zhang, Qing, Le Roy, Robert, Vandamme, Matthieu, & Zuber, Bruno. 2014.

Long-term creep properties of cementitious materials: Comparing microindentation testing with macroscopic uniaxial compressive testing. *Cement and Concrete Research*, **58**, 89–98.

Figure1
Click here to download Figure: Fig1-PrincipleMicroprestress.pdf

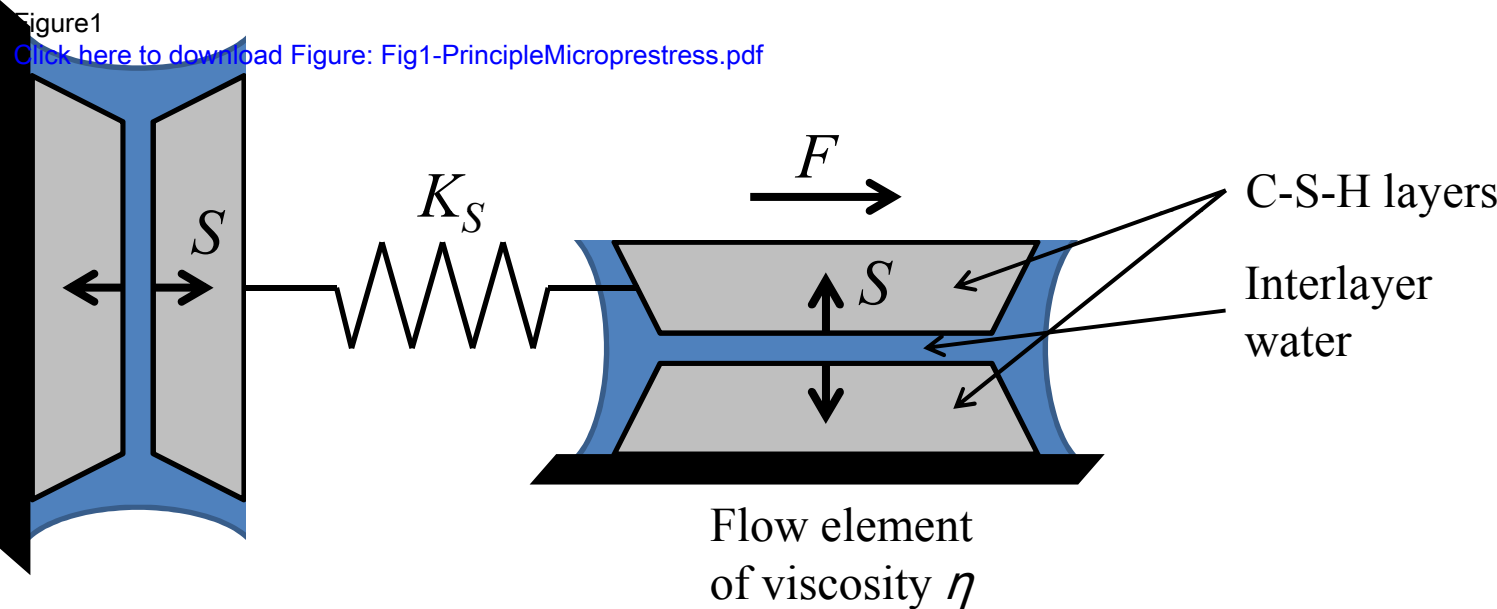

Figure2
Click here to download Figure: Fig2-System.pdf

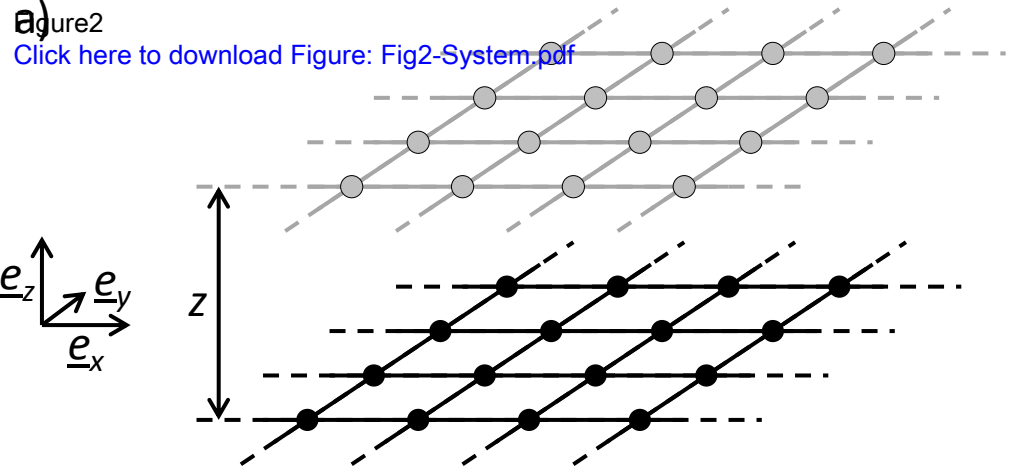

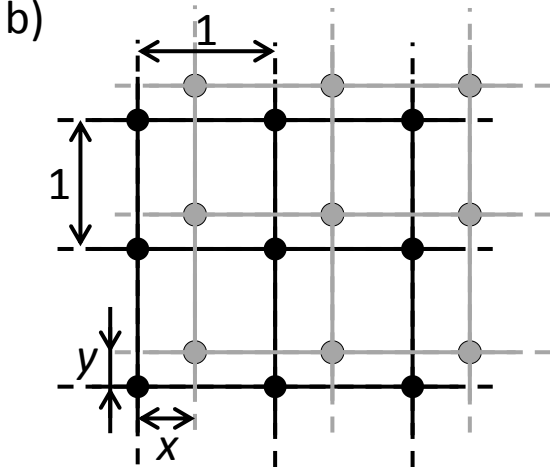

Figure3

Click here to download Figure: Fig3 Energy Landscape LJ 2D.pdf

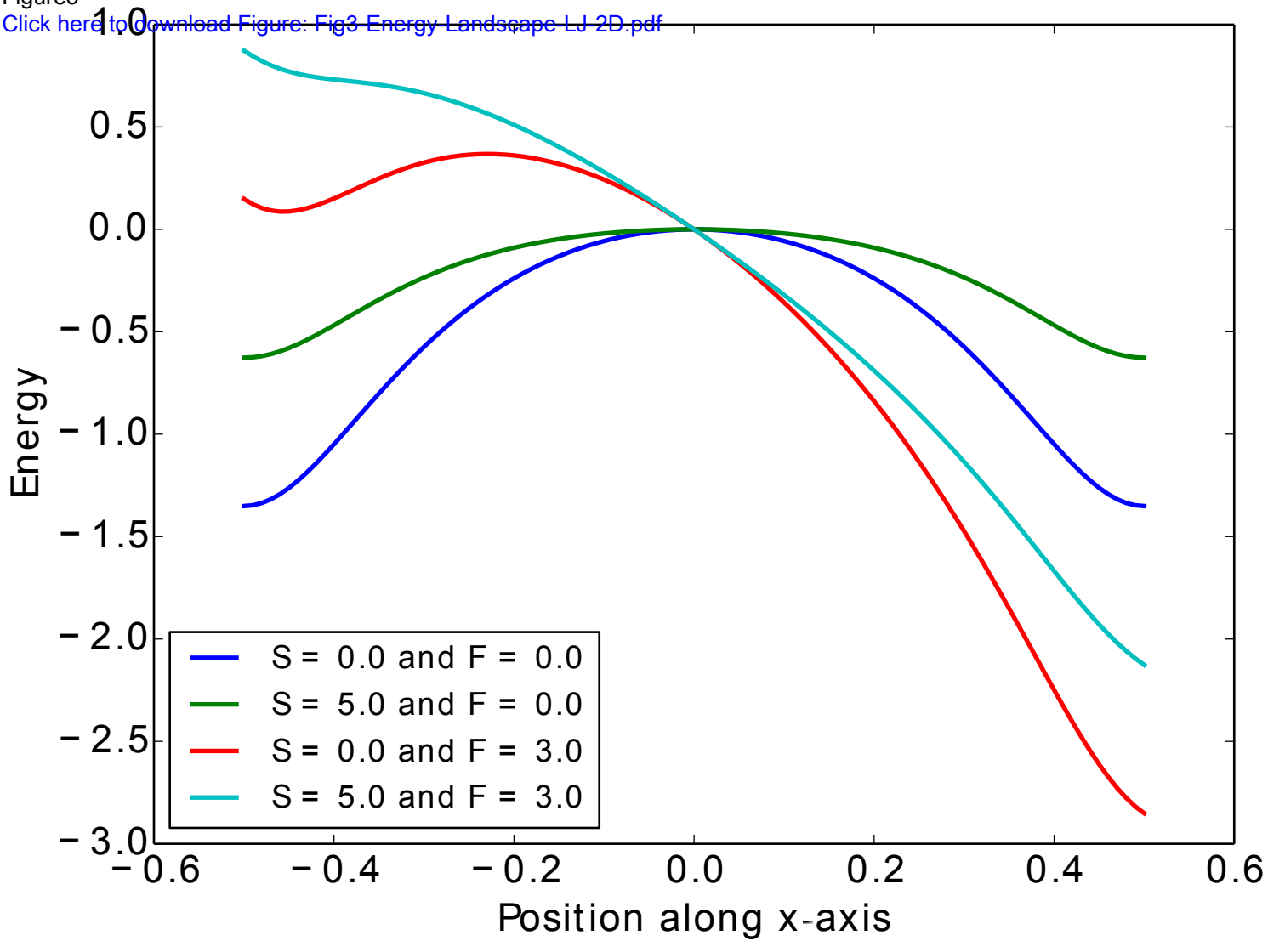

a)

Figure4

Click here to download Figure: Fig4-Energy-Barriers-Length1.pdf

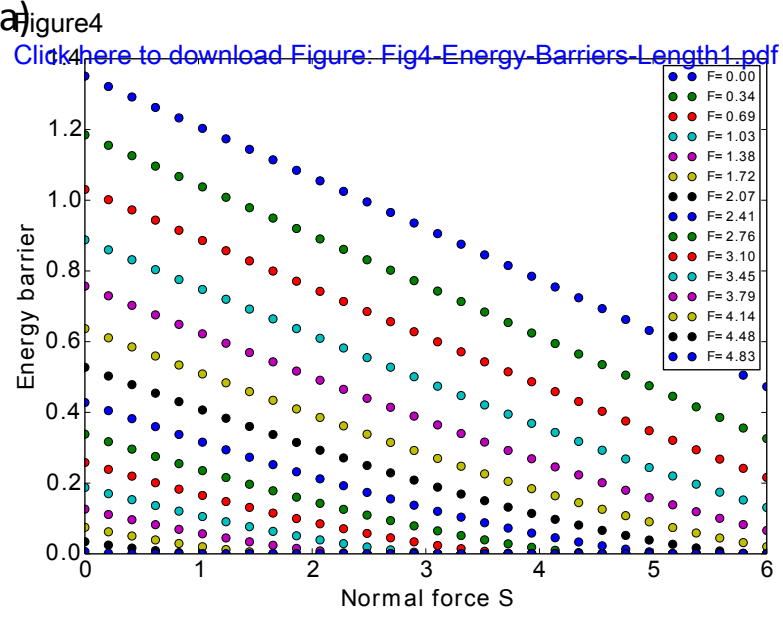

b)

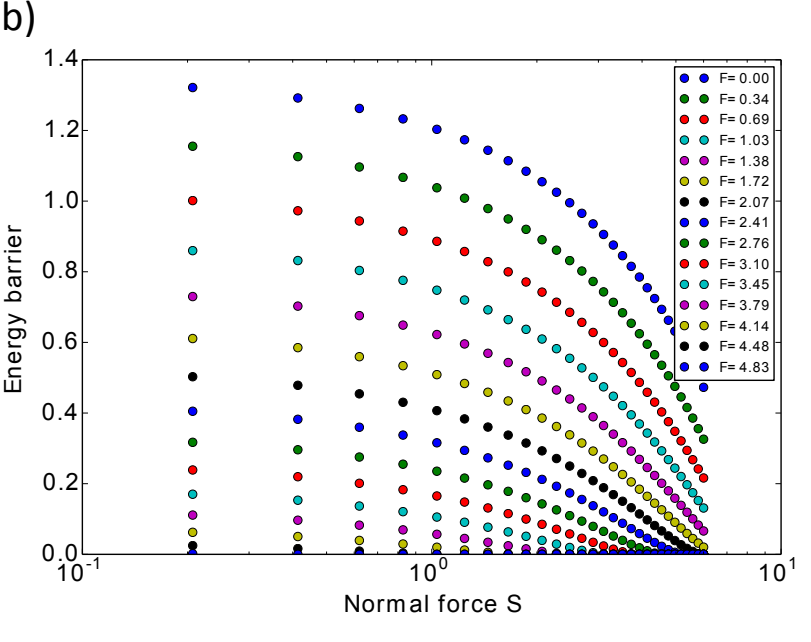

a) Figure5

Click here to download Figure: Fig5-Various-Water

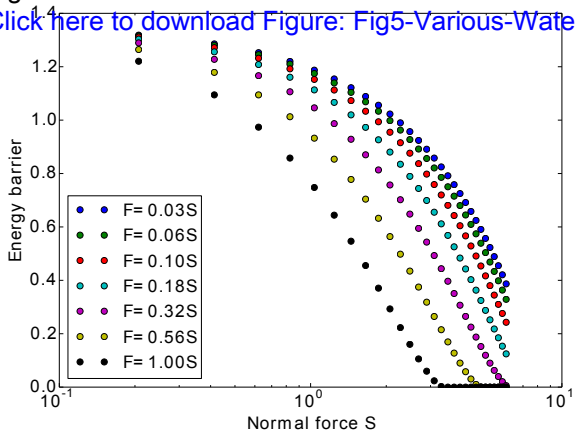

b)

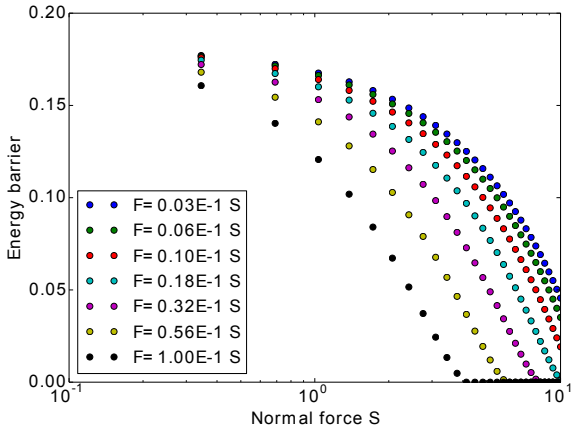

c)

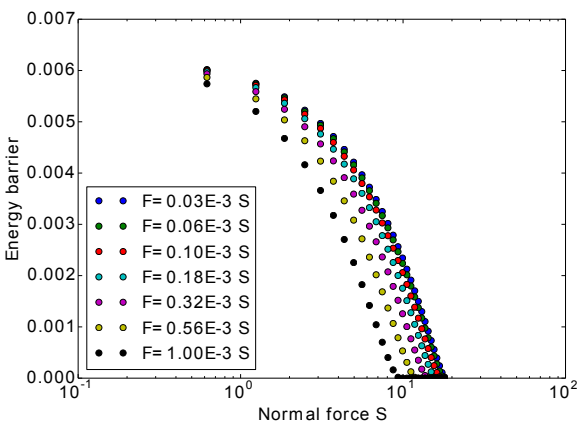

Figure6

a)

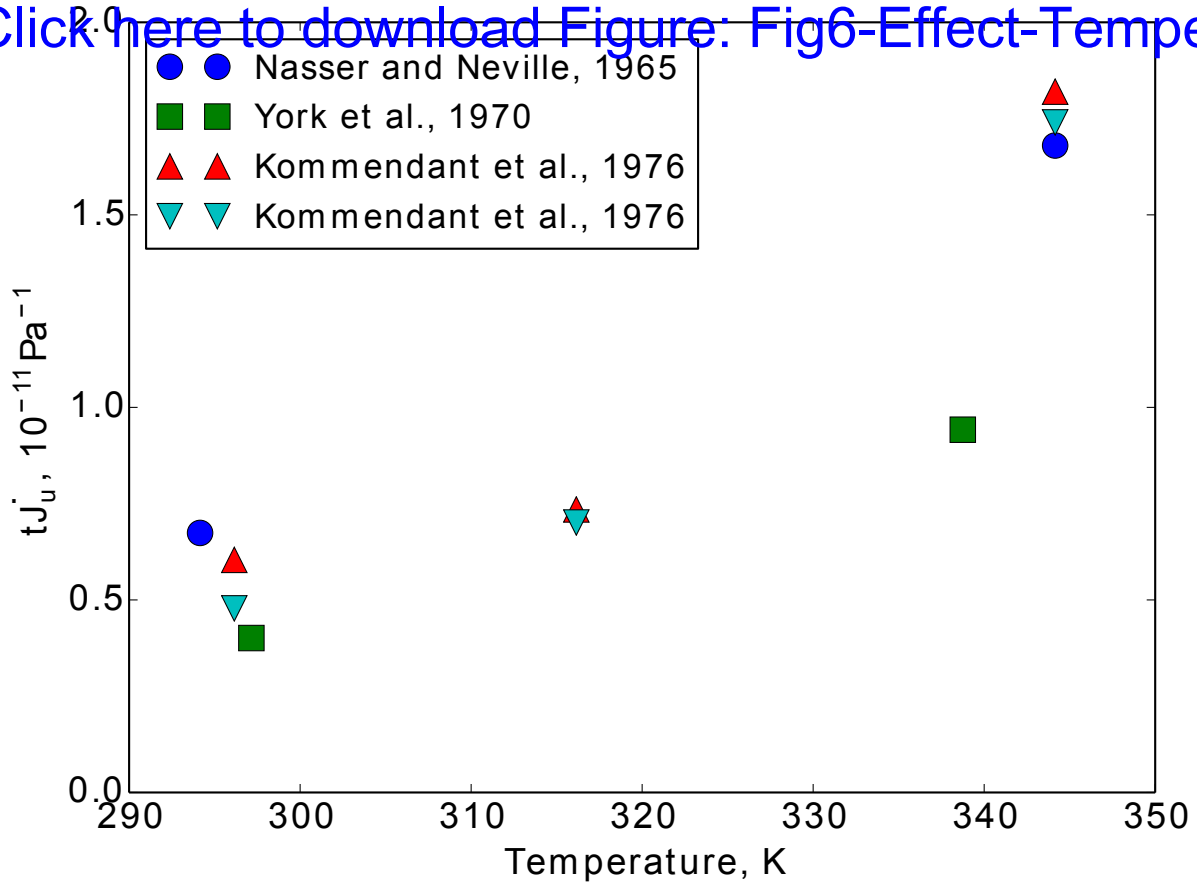

b)

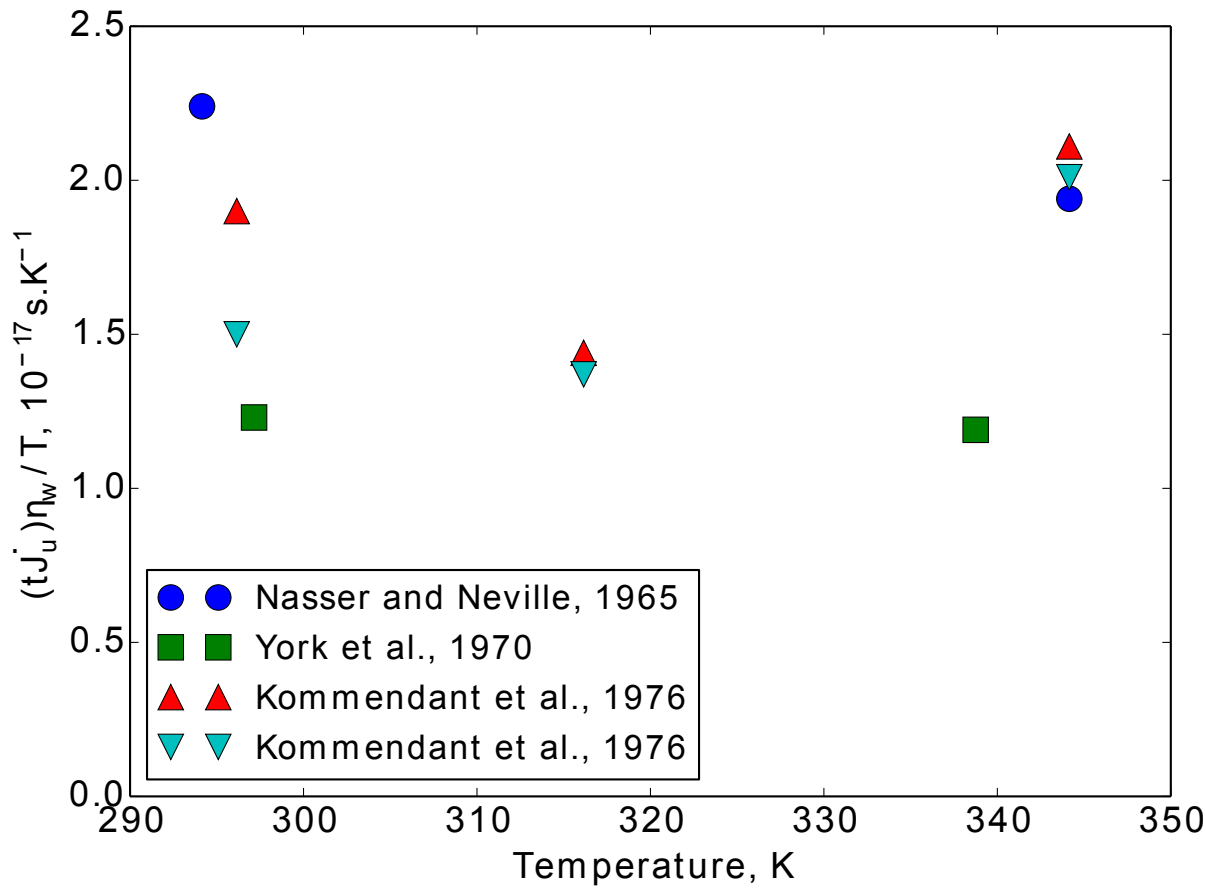

Figure7
Click here to download Figure: Fig7-Effect-Spacing.pdf

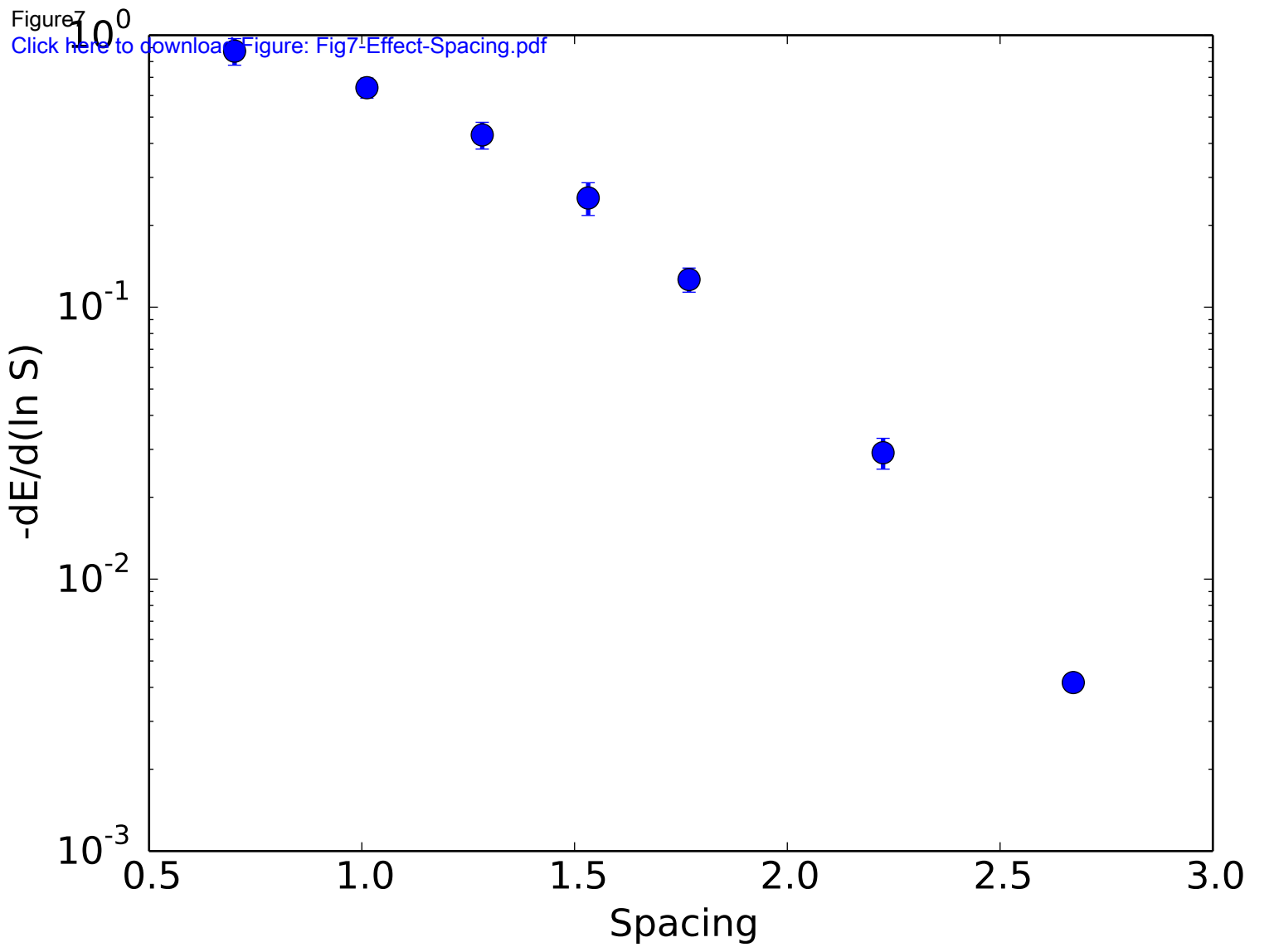

Figure8

Click here to download Figure: Fig8-Effect-Water-Content.pdf

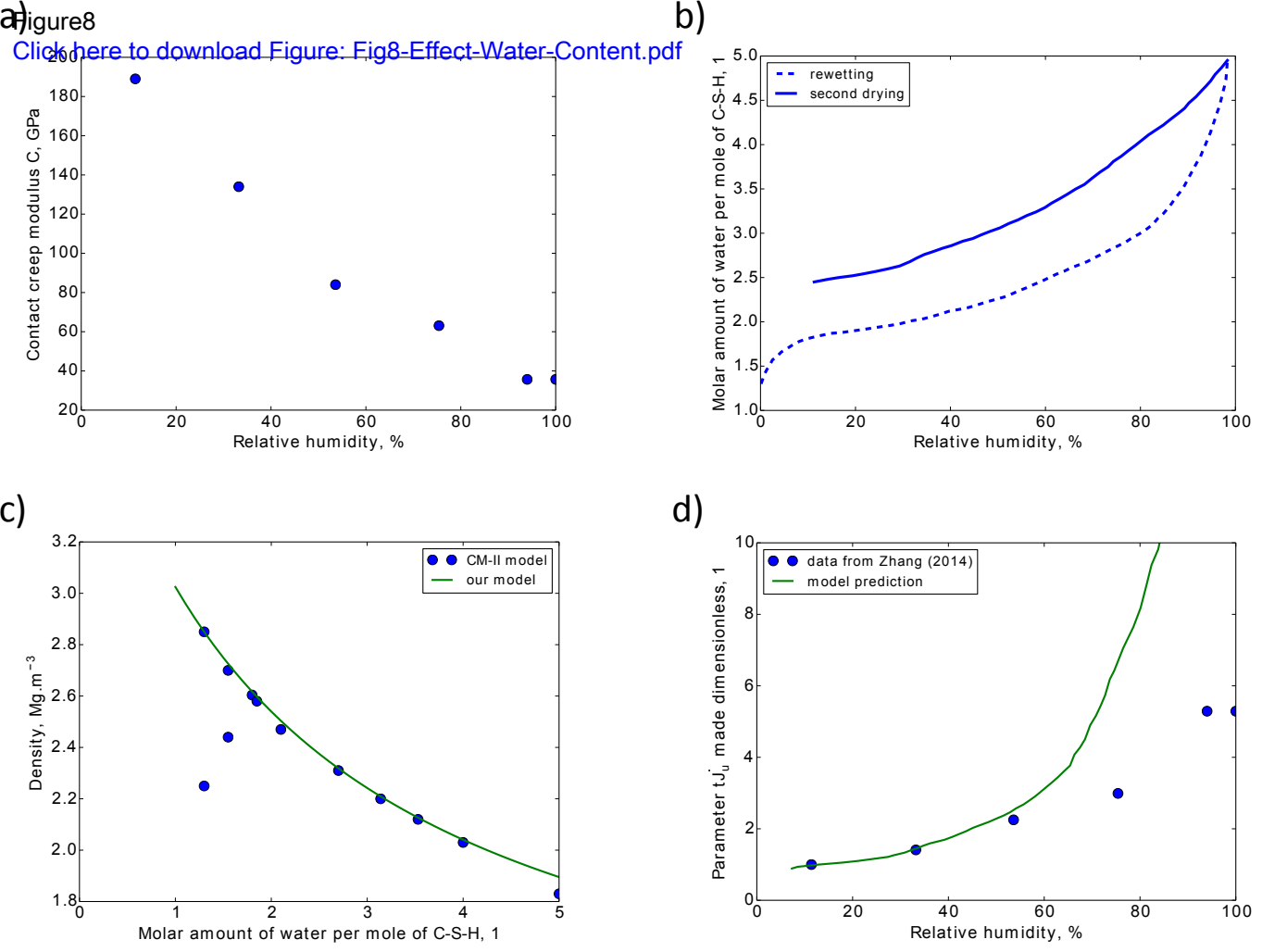

List of figure captions

Figure 1: Principle of the microprestress theory. Adapted from Bažant et al. (1997).

Figure 2: System considered: infinite parallel plates with a square lattice: a) perspective view and b) view in the $\underline{e}_z$ direction. In-between the plates, one finds out the interlayer fluid, modeled as a continuum and not represented on this figure.

Figure 3: Energy landscape explored by the system upon sliding of the two plates over each other, under the action of a microprestress S and of a transversal load F.

Figure 4: Energy barriers to the sliding over each other of infinite rigid plates interacting through Lennard-Jones potential, plotted on a) a linear scale and b) a logarithmic scale.

Figure 5: Energy barriers for the transversal motion of infinite rigid plates interacting through Lennard-Jones potential, when the transversal force F is considered to be a fraction of the microprestress S. Calculations were performed for equilibrium spacing equal to: a) $r_0=1$, b) $r_0=2$, and c) $r_0=3$.

Figure 6: Effect of temperature T on a) parameter $c_u = t \dot{J_u}$ and b) parameter $t \dot{J_u} \eta_w / T$. The parameters $c_u = t \dot{J_u}$ are obtained by fitting experimental creep

data on concrete specimens, which can be found in Bažant et al. (2004) and were obtained by Nasser and Neville (1965), York et al. (1970), and Kommendant et al. (1976). The data by Kommendant et al. were obtained by loading the specimens after 28 days of hydration (upward triangles) and after 90 days of hydration (downward triangles).

Figure 7: Effect of basal spacing on how the energy barrier depends linearly on the logarithm of the microprestress S.

Figure 8: Effect of relative humidity on properties of C-S-H. a) Effect of relative humidity on contact creep modulus of C-S-H, measured by microindentation by Zhang (2014). b) Adsorption isotherm of C-S-H upon rewetting and second drying (adapted from Jennings (2008). c) Effect of water content on basal spacing, according to Jenning's CM-II model (Jennings, 2008), and as predicted by our geometrical calculation. d) Effect of humidity on parameter $c_u = t \dot{J_u}$ made dimensionless, as back-calculated from the results of Zhang (2014) and as predicted by our model.